RESEARCH ARTICLE | MAY 03 2023

Synthesis and characterizations of $LiMn_2O_4$ sheet over Al foil as cathode material for Li ion battery

Deswita Deswita; Yulia Indriani; Indra Gunawan; ... et. al

AIP Conference Proceedings 2517, 020011 (2023)
https://doi.org/10.1063/5.0121499

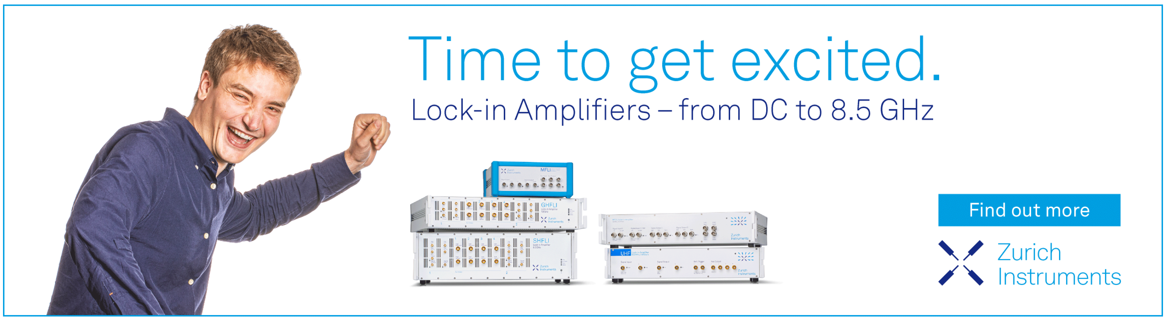

Synthesis and Characterizations of $LiMn_2O_4$ Sheet over Al Foil as Cathode Material for Li Ion Battery

Deswita Deswita[1, a)], Yulia Indriani[2], Indra Gunawan[1, b)], Sudaryanto Sudaryanto[1], Evvy Kartini[1, 3]

[1]*Centre for Advanced Materials Science and Technology, National Nuclear Energy Agency Bld. 71 PUSPIPTEK-15314 Serpong, Indonesia*

[2]*Faculty of Mathematics and Natural Science, Universitas Sebelas Maret – 57126 Surakarta, Indonesia*

[3]*National Battery Research Institute, 2nd Floor EduCenter Building Unit 22260 BSD, South Tangerang 15314, Indonesia*

[a)] *Corresponding author: deswita@batan.go.id*
[b)] *irgun.ig@gmail.com*

Abstract. The synthesis of $LiMn_2O_4$ cathode was began by manufactured a slurry with consisting of 90% $LiMn_2O_4$, 5% Acetylene Black (AB) and 5% PVDF. The sample was dissolved in 3 ml of NMP solution that had been mixed with 5% PVDF, then stirred with a vacuum mixer for 15 minutes until the sample become a slurry. The slurry is placed on top of aluminum foil to be used as a cathode using a dactor blade. Characterization was done using XRD, PSA, SEM and LCR meter. It was found that the diffraction peaks were the strongest in the $LiMn_2O_4$ powder sample. The average particle size of $LiMn_2O_4$ is in the range between 214.64 nm - 318.18nm. The $LiMn_2O_4$ cathode is seen if there are nets that bind between the particles which is caused by the addition of PVDF polymer. So that PVDF causes one particle to bind to another, which will create gaps in the $LiMn_2O_4$ cathode. The conductivity of $LiMn_2O_4$ was obtained of about 3.00×10^{-5} $S.cm^{-1}$.

INTRODUCTION

Batteries are divided into 2 types, namely primary batteries and secondary batteries. The primary battery is used only once and cannot be recharged, due to an irreversible electrochemical reaction. In contrast, secondary batteries, also called rechargeable batteries, are electrochemical batteries that can be reused cyclically by discharging and recharging. This is because the electrochemical reaction is reversible. The development of secondary batteries has increased rapidly, including the development of secondary batteries for nickel-metal hydride batteries, lithium-ion batteries, and sodium-ion batteries [1]. Among the secondary batteries, lithium-ion batteries commonly known as Li-ion batteries or LIBs exhibit high energy density and excellent working performance. In addition, Li-ion batteries are lighter in weight and have a longer cycle time than the previous generation secondary batteries. Because batteries have a very important role as a power source in technological innovation, Li-ion batteries are also a suitable choice so that they can lead other secondary batteries and have been widely used in various fields such as being used in communication equipment, portable equipment to electric vehicles [2][3]. Li-ion batteries are experiencing rapid and innovative development due to the increasing market demand that requires better and cheaper materials, especially the electrode materials. Li-ion batteries use an intercalated lithium compound as the electrode material, in contrast to the metallic lithium used in non-rechargeable lithium batteries [4][5]. This battery is the most popular type of rechargeable battery for portable electronic equipment, as it has one of the best energy densities, has no memory effect, and experiences slow charge loss when not in use. In addition to being used in consumer electronic equipment, Li-ion batteries are also often used by the military, electric vehicles, and aerospace industries. Numerous studies seek to improve the technology of traditional Li-ion batteries, focusing on energy density, durability, cost and intrinsic safety [3][6][7]. The next-generation Li-ion battery is expected to not only have high power, high capacity, high charge rate, long life, but also dramatically improve safety performance and low cost [8].

A basic Li-ion cell consists of a cathode (positive electrode) and anode (negative electrode) which are contacted by an electrolyte containing lithium ions [9]. The electrodes are isolated from each other by a separator which allows the exchange of lithium ions between the two electrodes. Li-ion battery cell operation has a distinctive principle [1][10]. During the charging process, the two electrodes are externally connected to an external power supply. The

The International Conference on Battery for Renewable Energy and Electric Vehicles (ICB-REV) 2021
AIP Conf. Proc. 2517, 020011-1–020011-7; https://doi.org/10.1063/5.0121499
Published by AIP Publishing. 978-0-7354-4444-7/$30.00

electrons are forced to be released at the cathode and move externally to the anode [11]. Simultaneously, the Li+ ions move in the same direction, but internally, from the cathode to the anode through the electrolyte. In this way the external energy is stored electrochemically in the battery. On the other hand, during the discharging process, electrons move from anode to cathode through an external load which must act and Li+ ions move from anode to cathode in the electrolyte [12].

Therefore, in this study the author will examine the electrodes for Li-ion batteries, especially on the cathode material. This is because $LiMn_2O_4$ has abundant manganese resources and this material can be easily obtained. Moreover, this material does not involve the use of toxic metal elements. All these advantages can promote the large-scale application of $LiMn_2O_4$. Therefore, further analysis of $LiMn_2O_4$ is needed to improve battery performance.Since the performance of Li-ion batteries is largely determined by the quality of the cathode material, so the cathode material is being actively developed and the cathode fabrication technology is being improved. The manufacture of this Li-ion battery cathode will go through a characterization stage using XRD, PSA, SEM/EDS and LCR Meter. Because of the nature of the material, it is very important to understand the relationship between battery material and battery quality before cell assembly is carried out. The active material used for the cathode in this study is LiMn2O4.

METHODOLOGY

Sample Preparation the materials used for the sample preparation of $LiMn_2O_4$ sheet were, commercial $LiMn_2O_4$ (2.7 grams), serves as the active material used. Acetylene Black (AB) (0.15 gram), serves as a carbon-based conductive material. NMP+PVDF (3 ml), NMP functioned as sample solvent and PVDF as binder. Aluminum Foil (1 sheet), serves to be coated with slurry. Alcohol, serves as a tool cleaner to be used.

The manufacture of $LiMn_2O_4$ cathode begins with preparing a slurry composition consisting of 90% $LiMn_2O_4$, 5% Acetylene Black (AB) and 5% PVDF. 2.7 grams of $LiMn_2O_4$ and 0.15 grams of AB were ground for 1 hour. Then put in a Hasuc vacuum oven at 100ºC for 6 hours. Then the sample was ground again for 20 minutes. After that, the sample was dissolved in 3 ml of NMP solution that had been mixed with 5% PVDF. Then stirred with a vacuum mixer for 15 minutes until the sample is like a sweet viscous called a slurry. The aluminum foil is vacuumed over the doctor blade and cleaned with alcohol first. Then the slurry is placed on top of aluminum foil to be used as a cathode using a dactor blade with a thickness of 150 microns. Then the cathode was put into a vacuum oven for 2 hours at 80ºC. Then it is molded into a circle shape for the coin battery cathode.

Characterization

$LiMn_2O_4$ cathode was characterized using XRD, PSA, SEM/EDS and LCR Meter. XRD serves to ensure that the sample used is based on the diffractogram and determines the crystal phase. Then PSA serves to determine the particle size quantitatively. SEM serves to observe the microstructure of the sample. The $LiMn_2O_4$ sample was tested for microstructure by coating with Au first in order to produce a clearer image. SEM test was carried out for samples of $LiMn_2O_4$ active material, LiMn2O4 cathode and cathode without active material (AB+NMP+PVDF only). EDS is a complementary SEM device that serves to determine the composition in the sample. The samples used are $LiMn_2O_4$ active material and $LiMn_2O_4$ cathode. The last characterization is the LCR Meter which is used to measure the conductivity of the $LiMn_2O_4$ cathode.

RESULTS AND DISCUSSION

In this study will discuss more deeply about the positive electrode (cathode). The active material used in the manufacture of the cathode is $LiMn_2O_4$. The manufacture of this $LiMn_2O_4$ cathode uses a composition ratio of 90%:5%:5% $LiMn_2O_4$:AB:PVDF. At first, $LiMn_2O_4$ and AB were ground for 1 hour to homogenize the two. Then heated using a vacuum oven for 100ºC for 6 hours which serves to evaporate the oxide contained in the sample. Furthermore, the sample was ground again and dissolved into the NMP solution containing 3 ml of PVDF. The NMP+PVDF solvent that has been used has a yellow color which according to the 2017 Puspita journal, heating gives a yellowish color to the resulting solution which may be caused by an oxidation reaction or the formation of conjugate bonds in the PVDF polymer. The higher the heating temperature, the darker the yellow color produced. NMP is used as a solvent and PVDF is a polymer that functions to bind particles to one another. Then the sample is stirred using a vacuum mixer to form a slurry. Slurry is smeared on aluminum foil to be used as a cathode using a doctor blade with a size of 150 microns. The $LiMn_2O_4$ cathode was heated using a vacuum oven for 2 hours at 80ºC to evaporate the

NMP. After that the cathode is cut into the form of a coin cell cathode, After that, the LiMn2O4 cathode characterization test was carried out.

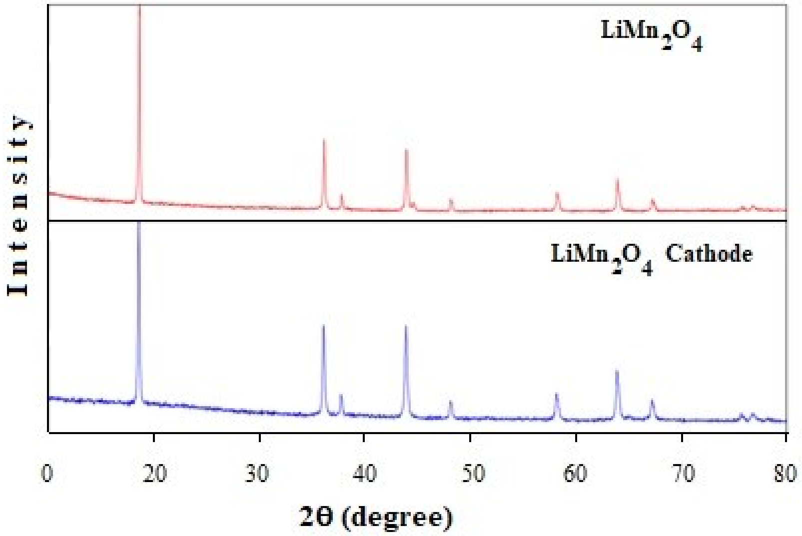

FIGURE 1. XRD patern of LiMn$_2$O$_4$ powder (a) and LiMn$_2$O$_4$ sheet (b).

The characterization test with XRD was carried out using 2 samples, namely LiMn$_2$O$_4$ powder samples and LiMn$_2$O$_4$ cathodes. Figure 1 shows a graph of the relationship between intensity and 2θ in both samples. XRD data is taken from an angle of 10º-80º, The anode used is Cu with a wavelength of 1.54 . Based on the Cristalography Open Data base (COD) data base, it was found that the diffraction peaks at 8 angles of 2θ were the strongest in the LiMn$_2$O$_4$ powder sample, namely 18.675º; 36,330º; 37.906º; 44,097º; 48.262º; 58,280º; 64.133º and 67.398º. While at the LiMn$_2$O$_4$ cathode there are 8 strongest 2θ angles, namely 18,586º; 36,153º; 38.049º; 44.116º; 48,160º; 58,271º; 63,958º; and 67,245º. The detected peaks are almost the same with each other and the COD data base is almost the same. So that the elements detected in the sample are the same. The peaks formed belong to the elements Li, Mn and O in both samples. So that in the LiMn$_2$O$_4$ cathode sample the content remains even though there is a process where AB and PVDF are added. This is because AB is amorphous and PVDF is semicrystalline so XRD cannot detect elements from the addition of the two. However, on the LiMn$_2$O$_4$ powder graph there is an additional 1 peak where the element cannot be determined because there is only 1 additional peak. This additional peak is at 44.615º. This is because the LiMn$_2$O$_4$ powder used is a commercial LiMn$_2$O$_4$ so it is difficult to interpret the additional elements. The crystal structure obtained from the sample is in the form of a simple cubic. In the graph above, it can be seen that the intensity of the LiMn$_2$O$_4$ powder is greater than that of the LiMn$_2$O$_4$ cathode. This is because at the LiMn$_2$O$_4$ cathode there are several treatments such as heating and grinding that allow a change in crystal orientation when XRD is carried out so that there is a decrease in intensity.

LiMn2O4 powder was characterized using PSA to determine the particle size in detail and determine the size distribution distribution. In Figure 2, it can be seen that if there are 3 peaks with the first peak (the highest) there are particles with a size of 176 nm as much as 85.3%, the second peak with particles measuring 9.825 nm as much as 13.4% and the lowest peak with 4861 nm particles as much as 1.3%. . So that the average particle size in PSA is 214.64 nm with the largest size being 176 nm.

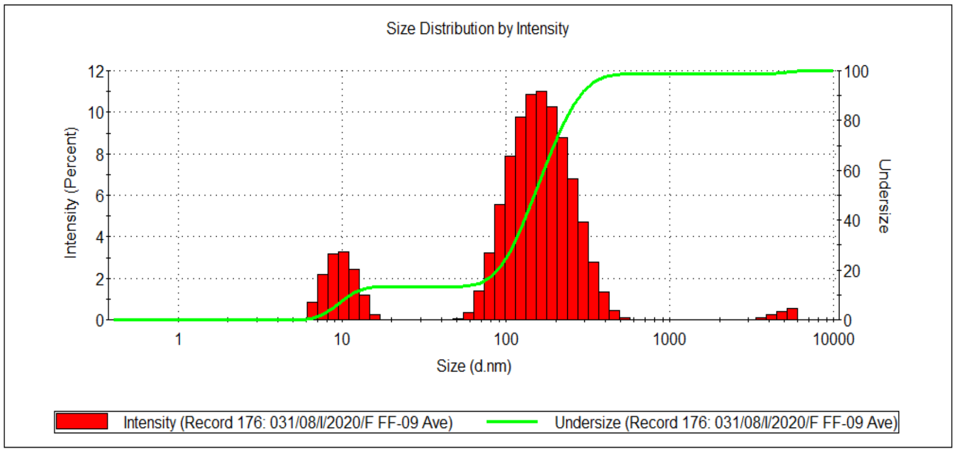

FIGURE 2. $LiMn_2O_4$ powder was characterized using PSA.

SEM tests were carried out for the active material, $LiMn_2O_4$ cathode and cathode without active material (AB+NMP+PVDF only). All samples were characterized by SEM with Au coated and without Au coating where the results will be clearer on Au coated samples. The Au-coated $LiMn_2O_4$ powder will be more clearly visible than the uncoated LiMn2O4 powder, as shown in Figure3. The particle gaps in Figure 3a are more clearly visible. Meanwhile, in the sample without coating, it is seen that the particles accumulate between each other. This is because the Au-coated $LiMn_2O_4$ sample will be more conductive so it will be easier to observe by SEM. Au coating is done using sputtering. Au was chosen because of its high conductive properties. In non-conductive samples, for 0-2000x magnification without Au coated and with low vacuum, SEM can still observe the morphology of the sample quite clearly. As for the magnification of more than 2000x, the sample must be coated to make it more clearly visible. In Figure 4.4 it can be seen that the particles of $LiMn_2O_4$ powder have a shape mostly like a pyramid. In Figure 4.4b, there is a white part of the collection of particles (cannot be clearly observed by SEM) which is called charging. Then the comparison for the $LiMn_2O_4$ cathode sample with Au coating and without coating which has the following image.

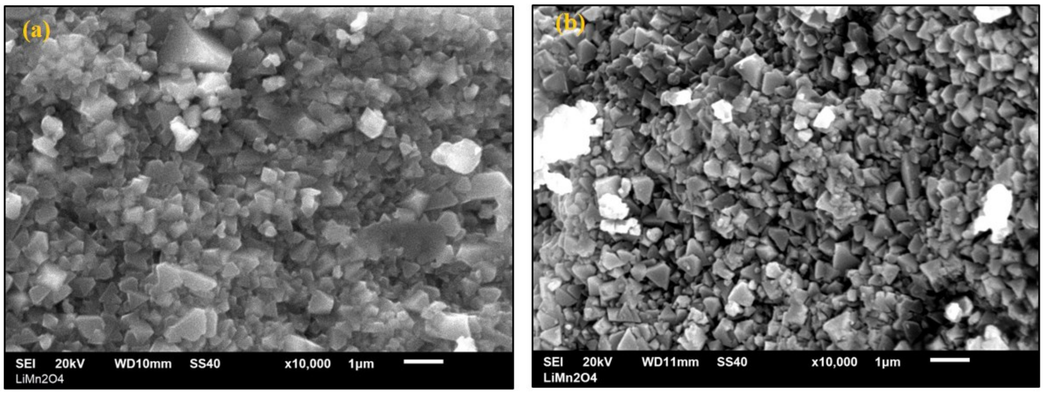

a **B**

FIGURE 3. SEM display of (a) $LiMn_2O_4$ powder without Au coating (b) $LiMn_2O_4$ powder with Au coating

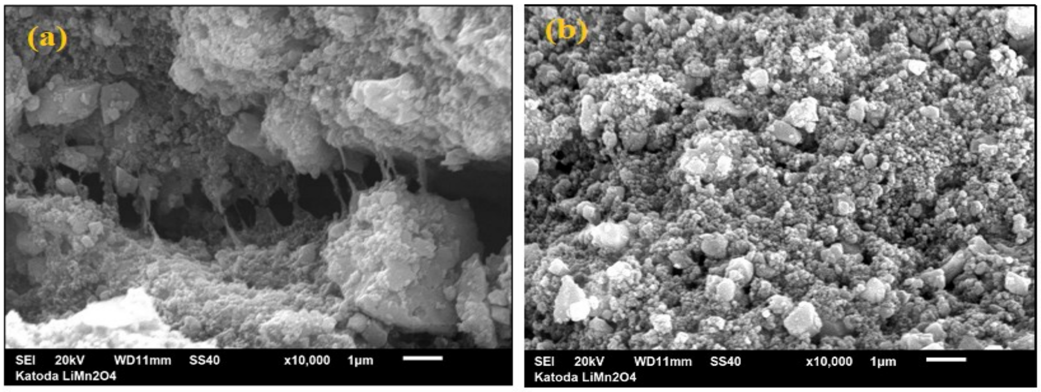

FIGURE 4. $LiMn_2O_4$ cathode SEM 10,000x display at different positions

In Figure 4a, it can be seen that there are nets that bind between the particles. The nets are caused by the addition of PVDF polymer. So that PVDF causes one particle to bind to another, which will create pores on the $LiMn_2O_4$ cathode as shown in Figure 4b.

SEM devices are equipped with EDS or Energy Dispersive Spectroscopy. EDS is used to determine the chemical composition of the particles that make up the sample. The material characterization with EDS uses X-rays that are emitted when the material collides with electrons. The energy level depends on the energy level of the atomic shell, because X-rays are emitted from transitioning electrons from the atomic shell layer. So that by detecting the level of energy emitted from X-rays and their intensity, it can be seen the atoms making up the material and their mass percentage. In this study, the composition of EDS for $LiMn_2O_4$ powder samples was obtained as shown in Figure 5.

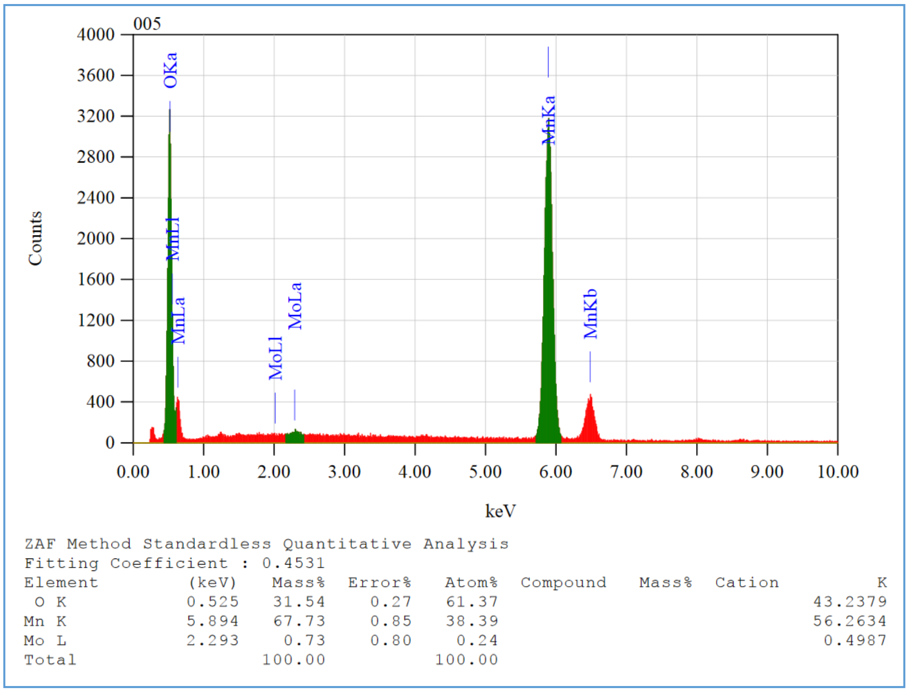

```
ZAF Method Standardless Quantitative Analysis
Fitting Coefficient : 0.4531
Element         (keV)    Mass%   Error%    Atom%  Compound    Mass%  Cation          K
 O K            0.525    31.54     0.27    61.37                               43.2379
Mn K            5.894    67.73     0.85    38.39                               56.2634
Mo L            2.293     0.73     0.80     0.24                                0.4987
Total                   100.00            100.00
```

FIGURE 5. EDS results of $LiMn_2O_4$ powder composition

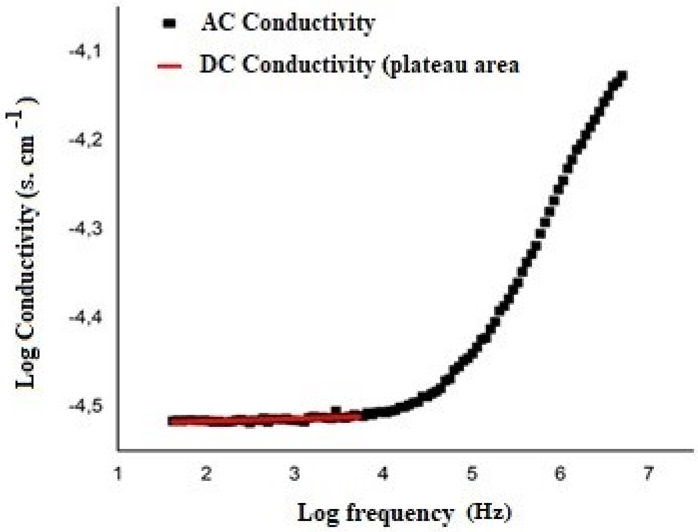

FIGURE 6. Graph of Log Conductivity Vs Log Frequency of Cathode $LiMn_2O_4$

Characterization using LCR Meter was carried out to measure the conductivity at the $LiMn_2O_4$ cathode. Changes in the conductivity value on the curve indicate the movement of Li+ ions. On the LCR Meter data obtained in the form of G and Frequency. Frequency here is a given energy response. Measurements were made with a sample thickness of 9.3x10-3 cm and the cross-sectional area of the sample used was 1.76625 cm. Processing is done with the help of Origin software. Based on the graph above, the magnitude of the DC conductivity (DC) is 3.003 x 10-5 S/cm.

CONCLUSION

The manufacture of $LiMn_2O_4$ cathode has been successfully carried out with a composition of 90%:5%:5% $LiMn_2O_4$:AB:PVDF. The materials used are mixed to form a slurry, then coated on an aluminum sheet as a substrate. Based on the Cristalography Open Data base (COD) data base, it was found that the diffraction peaks at 8 angles of 2θ were the strongest in the $LiMn_2O_4$ powder sample. The average particle size of $LiMn_2O_4$ using PSA is 214.64 nm, most of which are 176 nm. While the measurement of $LiMn_2O_4$ particles using SEM obtained an average of 318.18 nm. Through SEM, the $LiMn_2O_4$ cathode is seen if there are nets that bind between the particles. The nets are caused by the addition of PVDF polymer. Measurement of $LiMn_2O_4$ conductivity through LCR Meter obtained a conductivity of 3,003 x 10^{-5} S/cm.

ACKNOWLEDGMENTS

The authors thank to Head of the Centre for Advanced Materials Science and Technology for those who have supported the research. This research was supported by Program Riset Inovatif Produktif (RISPRO) Mandatori 2021.

REFERENCES

1. J.-Y. Luo, W.-J. Cui, P. He, and Y.-Y. Xia, “Raising the cycling stability of aqueous lithium-ion batteries by eliminating oxygen in the electrolyte.,” *Nat. Chem.*, vol. 2, no. 9, pp. 760–5, 2010.
2. S. Ma, M. Jiang, P. Tao, C. Song, J. Wu, and J. Wang, “Progress in Natural Science : Materials International Temperature e ff ect and thermal impact in lithium-ion batteries : A review,” vol. 28, no. October, pp. 653–666, 2018.

3. M. Lachal *et al.*, “Remarkable impact of grains boundaries on the chemical delithiation kinetics of LiFePO4,” *Solid State Ionics*, vol. 300, pp. 187–194, 2017.
4. P. G. Pereirinha and A. Santiago, “Set up and test of a LiFePO 4 battery bank for electric vehicle,” Coimbra, Portuguese, 2012.
5. M. Safari, M. Farkhondeh, M. Pritzker, M. Fowler, T. Han, and S. K. Chen, “Simulation of lithium iron phosphate lithiation/delithiation: Limitations of the core-shell model,” *Electrochim. Acta*, vol. 115, pp. 352–357, 2014.
6. S. Yang, Y. Song, K. Ngala, P. Y. Zavalij, and M. Stanley Whittingham, “Performance of LiFePO4 as lithium battery cathode and comparison with manganese and vanadium oxides,” *J. Power Sources*, vol. 119–121, pp. 239–246, 2003.
7. C. Masquelier, A. K. Padhi, K. S. Nanjundaswamy, and J. B. Goodenough, “New Cathode Materials for Rechargeable Lithium Batteries: The 3-D Framework Structures Li3Fe2(XO4)3(X=P, As),” *J. Solid State Chem.*, vol. 135, no. 2, pp. 228–234, 1998.
8. G. E. Blomgren, J. E. Soc, and G. E. Blomgren, “The Development and Future of Lithium Ion Batteries The Development and Future of Lithium Ion Batteries,” 2017.
9. X. He *et al.*, “Charge/discharge characteristics of sulfur composite cathode materials in rechargeable lithium batteries,” *Electrochim. Acta*, vol. 52, no. 25, pp. 7372–7376, 2007.
10. Y. Xia, W. Zhang, H. Huang, Y. Gan, J. Tian, and X. Tao, “Self-assembled mesoporous LiFePO4 with hierarchical spindle-like architectures for high-performance lithium-ion batteries,” *J. Power Sources*, 2011.
11. E. H. Mohan, V. Siddhartha, R. Gopalan, T. N. Rao, and D. Rangappa, “Urea and sucrose assisted combustion synthesis of LiFePO 4 / C nano-powder for lithium-ion battery cathode application,” *AIMS Mater. Sci.*, vol. 1, no. 4, pp. 191–201, 2014.
12. N. H. Kwon *et al.*, “Nanoparticle shapes of LiMnPO4, Li+ diffusion orientation and diffusion coefficients for high volumetric energy Li+ ion cathodes,” *J. Power Sources*, vol. 342, pp. 231–240, 2017.